

Magnetite (Fe₃O₄)-filled carbon nanofibers as electro-conducting/superparamagnetic nanohybrids and their multifunctional polymer composites

Arindam Das · Muhammad Raffi ·
Constantine Megaridis · Despina Fragouli ·
Claudia Innocenti · Athanassia Athanassiou

Received: 1 March 2014 / Accepted: 30 December 2014 / Published online: 11 January 2015
© Springer Science+Business Media Dordrecht 2015

Abstract A mild-temperature, nonchemical technique is used to produce a nanohybrid multifunctional (electro-conducting and magnetic) powder material by intercalating iron oxide nanoparticles in large aspect ratio, open-ended, hollow-core carbon nanofibers (CNFs). Single-crystal, superparamagnetic Fe₃O₄ nanoparticles (10 nm average diameter) filled the CNF internal cavity (diameter <100 nm) after successive steps starting with dispersion of CNFs and magnetite nanoparticles in aqueous or organic solvents, sequencing or combining sonication-assisted

capillary imbibition and concentration-driven diffusion, and finally drying at mild temperatures. The influence of several process parameters—such as sonication type and duration, concentration of solids dispersed in solvent, CNF-to-nanoparticle mass ratio, and drying temperature—on intercalation efficiency (evaluated in terms of particle packing in the CNF cavity) was studied using electron microscopy. The magnetic CNF powder was used as a low-concentration filler in poly(methyl methacrylate) to demonstrate thin free-standing polymer films with simultaneous magnetic and electro-conducting properties. Such films could be implemented in sensors, optoelectromagnetic devices, or electromagnetic interference shields.

Electronic supplementary material The online version of this article (doi:[10.1007/s11051-014-2856-6](https://doi.org/10.1007/s11051-014-2856-6)) contains supplementary material, which is available to authorized users.

A. Das · M. Raffi · C. Megaridis (✉)
Department of Mechanical and Industrial Engineering,
University of Illinois at Chicago, 842 West Taylor Street,
Chicago, IL 60607, USA
e-mail: cmm@uic.edu

M. Raffi
Plasma Research and Applications Laboratory, Islamabad,
Pakistan

D. Fragouli · A. Athanassiou
Smart Materials, Nanophysics, Istituto Italiano di
Tecnologia, Via Morego 30, 16163 Genova, Italy

C. Innocenti
INSTM Research Unit and Department of Chemistry,
Universita di Firenze, Via della Lastruccia 3,
50019 Sesto Fiorentino, Florence, Italy

Keywords Encapsulation · Conducting material ·
Superparamagnetic material · Carbon nanofiber ·
Hybrid material · Composite nanoparticle

Introduction

Many intriguing properties of hollow cylindrical structures filled with inorganic materials have motivated researchers to investigate such nanohybrids/nanocomposites in various areas of nanotechnology (Liu et al. 1999; Sloan et al. 1999; Dai et al. 1999; Kuzmany et al. 2001; Bachtold et al. 2001; Misewich et al. 2003), drug delivery and medical devices

(Charlier et al. 1996; Mönch et al. 2005), field ionization (Luo et al. 2011), electrochemistry (Day et al. 2005, 2007; Cheng et al. 2012), hydrogen storage (Costa et al. 2005), memory devices (Chou et al. 1994), sensors (Dong et al. 2007, 2008), nanoreactors (Wang et al. 2008; Castillejos et al. 2009; Palaniselvam et al. 2011), chemical probes (Winkler et al. 2006), catalysis (Pan and Bao 2008; Castillejos et al. 2009), etc. Carbon Nanotubes (CNTs) and Carbon Nanofibers (CNFs), among the most investigated cylindrical nanostructures (Dresselhaus et al. 2001), offer themselves as ideal platforms for studies in these areas. The term CNT is used herein to define *short* (up to a few microns) carbon tubular structures with nm diameter, while the term CNF is reserved for typically longer (several tens of microns) carbon tube structures with larger diameters of O(10 nm)–O(100 nm). The hollow cavity of CNFs and CNTs can be filled (Gautam et al. 2010) with other materials to synthesize a whole new class of nanohybrids that are well suited for specialized applications. Owing to their graphitic structure, CNTs and CNFs are most suitable for hosting metal or metal oxide nanoparticles (Gautam et al. 2010), magnetic nanoparticles (Gautam et al. 2010), fluorescent nanoparticles (Lee et al. 2008), polymers (Sinha-Ray et al. 2011), C₆₀ molecules (Smith et al. 1998, 1999), organic molecules (Take-nobu et al. 2003; Li et al. 2005), etc.

To design a novel nanosystem with desirable properties, it is often required to combine different intercalated nanomaterials, each with its own unique functionality. Nanocomposites with an encapsulated phase in a host material are expected to have chemical/physical protection and longer lifespan because the properties of each filling constituent in such nanohybrids can be retained or even enhanced upon containment within the host cylindrical structure. Additional properties or functionalities can be imparted by the nanoscale interaction between the host shell and the intercalated material. Several approaches have been reported so far to encapsulate various nanophase materials inside the hollow cavities of CNTs and CNFs. Metal-based materials have been added to the hollow cavities of CNTs and CNFs by arc discharge growth of carbon nanotubes (Guerretpiecourt et al. 1994; Demoncy et al. 1998), volatile metal complex filling and decomposition (Guan et al. 2005), capillary suction of molten metal salts (Ajayan and Iijima 1993; Tsang et al. 1994; Chu et al. 1996; Ebbesen 1996;

Ugarte et al. 1996), sonochemical fabrication and incorporation of magnetic nanomaterials inside the CNFs or other filling techniques. Although functionalization of outer and inner surfaces of CNTs/CNFs using organic chemistry techniques (Smith et al. 1998; Okazaki et al. 2001; Qiu et al. 2006; Tessonnier et al. 2009b) has allowed efficient filling with metal nanoparticles, the related methods are frequently complex and pose challenges when scaling up. In these studies, CNFs have several advantages, which include their relatively high electrical and thermal conductivities, thick/strong inert walls, wide commercial availability, etc.

Nanoparticles frequently exhibit size-dependent physical, thermal, electrical, and chemical properties (Goldstein et al. 1992; Brune et al. 2006). To overcome complications in interpreting measurements involving encapsulated particles with diverse sizes, recent CNT/CNF filling studies (Castillejos et al. 2009; La Torre et al. 2010, 2012) have intercalated monodisperse nanoparticles. CNFs are well suited for this approach because of their comparatively large hollow cavity (inner dia. much larger than a few nm), which allows the nanoparticles to invade more easily. On the other hand, the much longer CNF lengths hinder efficient packing of the intercalated particles throughout the entire CNF length, thus requiring additional processing steps (e.g. ultra-sonication). Encapsulation of magnetic nanoparticles in CNFs prevents oxidation or other chemical/physical modification, an advantage when such nanocomposite materials are targeted for electric or magnetic applications.

Nanostructured composites with magnetic properties have been attracting increased attention, as of recently. Sutradhar et al. (2013) reported a solvent-based sonochemical process to encapsulate superparamagnetic and ferrimagnetic nanoparticles in multi-walled carbon nanotubes. Other recent studies (Pati et al. 2010, 2012) employed nanoparticles of different materials which were mixed via wet-based chemical routes and sintered by heat to produce magnetic nanostructured composites. Magnetic nanoparticles encapsulated inside CNTs have also been reported by Tilmaciu et al. (2009), Gautam et al. (2010), and Wolny et al. (2010). Filling of CVD carbon fibers (dia. ~ 300 nm) has been reported by Gogotsi and co-workers (Korneva et al. 2005; Kornev et al. 2008), however, these large vessels featured fragile walls of amorphous carbon, thus could be vulnerable under harsh mechanical handling.

Recently, research articles have appeared on synthesizing gold (La Torre et al. 2012) and other metal (Tessonier et al. 2009a) nanoparticles *inside* CNF cavities using complex chemical routes, which result in low packing efficiencies.

The goal of this study is to fabricate and characterize a multifunctional (electro-conducting and magnetic) composite powder, and use it as filler in thin polymer films with the same functionalities. We present a nonchemical, mild-temperature technique to encapsulate magnetite (Fe_3O_4) nanoparticles into durable-wall, hollow-core CNFs by ultra-sonication-assisted capillary imbibition, and self-sustained diffusion. The latter was introduced by Bazilevsky et al. (2008) to intercalate macromolecules and nanoparticles in nanotubes. CNF filling is achieved by capillary imbibition and diffusion-driven concentration gradients established during solvent evaporation from particle-containing stable dispersions. The present approach achieves comparatively dense packing of metal nanoparticles inside the hollow cavities of the fibers. We perform a systematic study of the effects of important processing parameters and produce CNFs loaded with densely packed magnetite nanoparticles by careful control and optimization of process conditions. Such hybrid powders exhibit novel properties by combining the electric conductivity of the encasing CNFs, the mechanically durable structure of the CNF walls, and the magnetic properties of the intercalated nanoparticles. As a result, these novel materials may find applications as nanofillers in various polymeric systems. For example, inert polymeric matrices may be transformed into magneto- and electro-active functional metamaterials by incorporating these powders. Moreover, ordered assembly of the CNFs by weak external magnetic fields may result in polymeric nanocomposites with anisotropic physical properties (Fragouli et al. 2010; Erb et al. 2012; Fragouli et al. 2014). Furthermore, the magnetic CNFs can be used as principal components in magnetic-field-controlled sensors, opto-electro-magnetic devices, etc.

Experimental

Materials and processes

Commercially available hollow-core CNFs (PR24-XT-LHT, Pyrograf III, Pyrograf Products Inc., USA)

were employed in this study (Fig. 1). The CNFs were produced from pyrolytically stripped carbon nanofibers, which featured thick walls of poorly ordered pyrolytic carbon formed during the synthesis process. The poorly ordered walls were graphitized by the manufacturer by subsequent heat treatment at 1,500 °C, leading to quasi defect-free walls. Most of the CNFs used in this study were open-ended with mechanically strong wall structure. They had 100 nm average outer diameter and 10–30 micron length (reduced lengths from the as-received state after 10 min of bath sonication), while their inner diameters were in the range 25–90 nm.

Oil-based EMG-911 and water-based EMG-508 ferrofluids (Ferrotec Inc. USA) were used as source of single-crystal superparamagnetic magnetite (Fe_3O_4) nanoparticles (average diameter ~ 10 nm, range 7–15 nm), which were diluted in either toluene (99.9 % ACS Grade, Fisher Scientific), acetone or water. The magnetite nanoparticles in EMG-911 were functionalized during manufacturing with fatty-acid molecules to assist long-term stability. In the case of the water-based EMG-508 ferrofluid, a low molecular weight anionic surfactant was included as dispersant. In their as-received state, the EMG-911 and EMG-508 ferrofluids contained, respectively, 2 and 1.2 vol% magnetite nanoparticles. In order to compare the effect

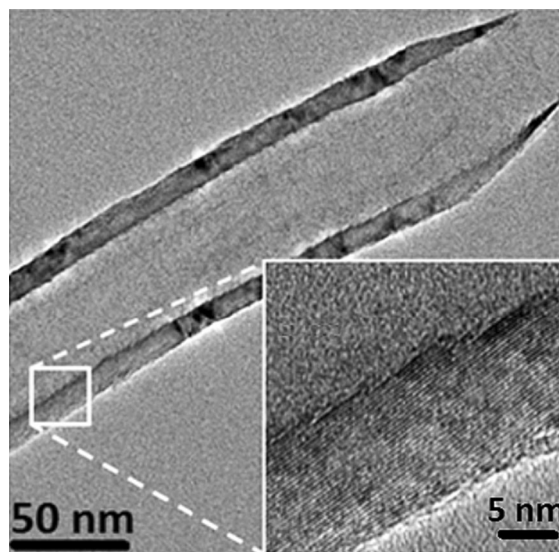


Fig. 1 HRTEM micrograph showing portion of a typical CNF used in this study. The exploded *inset* shows a magnified detail of the graphitic herringbone wall structure

of the nanoparticle functionalization to the CNF filling process, dry uncoated magnetite particle powders were also utilized; the characteristic dry particle size was 15–20 nm (NanoAmor, USA). Bath ultra-sonication (Cole-Parmer Model No: 08895-04, USA, 40 kHz, 70 W) and probe sonication (Sonics, Vibra-cell, Model VCX 750, 20 kHz, 750 W, 13 mm probe) were used to prepare the dispersions and facilitate the imbibition of the nanoparticles in the CNF cavities.

Dispersion procedures

For the base dispersions, 0.1–10 mg of CNFs was added in 20 ml liquid (toluene for oil-based ferrofluid, acetone, or water for water-based ferrofluid) and bath sonicated for 10 min. Subsequently, the appropriate magnetite nanoparticle-containing ferrofluid was added to the respective CNF dispersion either before or after the second sonication step, which featured either bath sonication or probe sonication (70 % amplitude), each maintained for a few seconds up to 360 min, as designated in the experiments intended to explore the influence of process parameters. In the case of probe sonication, the process was performed for 1 min at a time, to avoid excessive heating (and likewise evaporation losses) of the host liquid. After sonication, the dispersion was cooled for 1 min in room temperature water before the cycle was repeated, until the total sonication time reached the desired value. In the final dispersion, the CNF-to-nanoparticle mass ratio ranged from 2.5:1 to 10:1. To investigate the importance of nanoparticle functionalization, EMG-911 ferrofluid magnetite nanoparticles were substituted by the same amount of dry uncoated magnetite nanoparticles in toluene dispersions maintaining a 4:1 CNF-to-nanoparticle wt. ratio.

Drying of CNF/magnetite suspensions

The sonicated suspensions, as produced by the above-mentioned steps, were dried either at room temperature or at 120 °C (hotplate, Cimarec, USA) inside a chemical fume hood until all the solvent evaporated away. During this step, the solids concentration increased gradually, thus establishing particle concentration gradients from outside the CNFs to their less concentrated interior, in turn, driving the nanoparticles by diffusion into the CNFs (Bazilevsky et al. 2008). Upon complete drying, a black powder deposit

was obtained consisting of CNFs with magnetite nanoparticles both inside the CNF cavities and on the outer CNF walls. The latter necessitated an extra washing step to rid the CNF outer walls from nanoparticles adhered by molecular forces.

Washing of dried powder to remove nanoparticles from CNF exterior walls

The dried CNF-magnetite hybrids were subsequently re-suspended in toluene (when EMG-911 ferrofluid was used), or acetone or water (for EMG-508 ferrofluid) to remove the magnetite nanoparticles from the CNF outer surfaces by means of bath sonication. The effect of sonication time for the washing step was evaluated (in terms of removal of the exterior particles without apparent effect on the intercalated nanoparticles), and 10–15 min was found to be optimal. As such, this cleaning time was used in the experiments. Unless otherwise mentioned, 10 mg of CNF, 20 ml toluene, 4.16 mg of magnetite (in EMG-911 ferrofluid), and 120 °C drying temperature were used.

HRTEM characterization of magnetite-filled CNFs

Dilute dispersions (0.003 wt%) of nanoparticle-encasing CNFs with cleaned outer surfaces were deposited on lacey carbon, 300-mesh copper electron microscope grids. After drying, high-resolution (HR) image analysis was carried out in a JEOL-3010F (300 kV e-beam) transmission electron microscope (TEM). The filling efficiencies of CNFs obtained from different experiments were determined qualitatively from TEM images. HRTEM visualization was performed both in normal and tilt specimen modes. Tilt mode analysis (see Supporting Information) was required to distinguish whether the magnetite nanoparticles were encapsulated inside the CNFs or were attached to the exterior CNF wall surface.

Fabrication and characterization of CNF/PMMA nanocomposite films

CNFs intercalated with magnetite nanoparticles and washed to rid their outer walls from magnetite particle deposits were re-dispersed in toluene for further wet processing. PMMA (MW 120,000, Sigma Aldrich, USA) in toluene solution (concentration 100 mg/ml)

was mixed with the CNF/toluene dispersion to attain CNF:PMMA wt. ratio of 7.2 %. The final solution was drop-casted on glass slides ($1 \times 1 \text{ cm}^2$) and left to dry under ambient conditions, thus producing thin CNF/PMMA composite films.

For magnetic characterization of these films, a Quantum Design Ltd. SQUID (superconducting quantum interference device) magnetometer was used. The magnetization curves were acquired at room temperature, starting from an instrument magnetic field of 5 T and ramping down to zero. The temperature dependence of Zero-Field-Cooled and Field-Cooled (ZFC/FC) magnetization was measured under a static field of 5 mT after cooling the samples down to 5 K in a zero magnetic field (ZFC curve) or in the same probe field of 5 mT (FC curve). For the nanocomposite film, the data were corrected by the diamagnetic contribution of the PMMA polymer (control, measured separately). In all cases, the direction of the applied magnetic field is parallel to the plane of the substrates.

For film electronic conductivity measurements, a Keithley 2612A sourcemeter and a DL Instruments 1211 current preamplifier were used, both mounted on an ambient probe station (Süss Microtech, Germany). Samples were biased from 0 to -1 V , and from 0 to 1 V . Conductive silver paste electrodes were painted on the sample surfaces in order to minimize the contact resistance.

Results and discussion

Figure 1 shows a HRTEM image of a typical CNF used in this study. The micrograph reveals structural details of the walls, which consist of stacked cones of graphene layers at an angle to the fiber axis (herringbone structure). The stacked cones create a ratchet-like morphology along the CNF inner wall surface, which serves as an anchor for the nanoparticles entering the CNF channels. Due to their high degree of graphitization, the CNFs have high thermal and electrical conductivity (Al-Saleh and Sundararaj 2009). Moreover, their surface energy is $\sim 155 \text{ mN/m}$ (as per manufacturer's specifications), indicating a highly wettable surface. Wettability is important because it facilitates the intercalation of the nanoparticles into the CNFs from the host suspensions.

Intercalation of magnetic nanoparticles into the CNF cavities was performed via a physical solvent-

based process. Figure 2 shows a schematic of the entire intercalation process. Utilizing ultra-sonication, CNFs were first dispersed in the liquid medium. Magnetic nanoparticles were subsequently added (in the form of a ferrofluid) into this dispersion. The resulting nanoparticle/CNF dispersion was then ultrasonicated, followed by heating to completely evaporate the liquid. The dried deposit was finally re-dispersed into the same dispersion medium and bath sonicated for 10–15 min. This re-dispersion process helped to remove nanoparticles from the outside surface of the CNFs, while leaving the intercalated particles intact inside the CNF cavity (see Supporting Information).

The selection of the solvent/dispersion medium critically affects the particle intercalation efficiency. Ideally, a liquid with low surface tension and low viscosity is preferred, in order to readily pre-wet the CNF inner walls and carry the well-dispersed nanoparticles into the cavity. Based upon a series of experiments (see Supporting Information, Fig. S1) with different host liquids, toluene (surface tension 28.4 mN/m) was found to be the optimal dispersion medium.

Dispersibility of nanoparticles in the liquid host medium was another important criterion for effective filling of CNFs. Nanoparticles in a stably dispersed state (e.g., magnetite nanoparticles from EMG 911 ferrofluid) invaded the CNF cavity readily and in large numbers. On the other hand, nanoparticles which are not dispersible or hard to disperse in liquid showed very limited or no intercalation in the CNF cavity (See Supporting Information, Figs. S2 and S3). Hence, the effects of other process parameters were studied using easily dispersible nanoparticles (in EMG 911 ferrofluid) and toluene solvent.

Influence of process parameters

Further experimental efforts focused on how intercalation efficiency is affected by different process parameters, such as sonication type and duration, concentrations of CNFs and magnetite nanoparticles in the dispersion, and finally drying temperature.

Sonication type and duration

To investigate the influence of sonication type (bath vs. probe) on particle intercalation efficiency, two sets

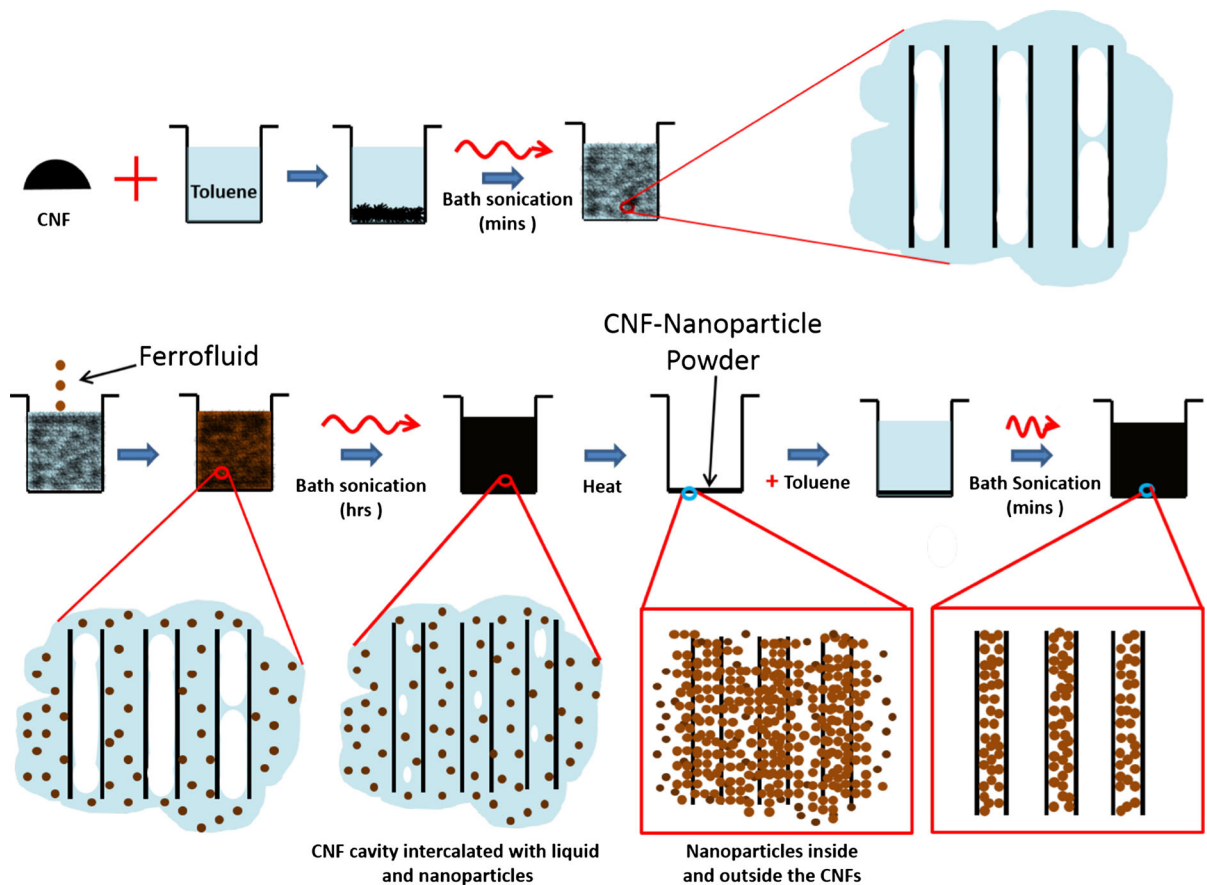


Fig. 2 Schematic of the processing steps used to intercalate Fe_3O_4 (magnetite) nanoparticles into hollow-core carbon nanofibers (CNFs). Light blue indicates liquid, while the brown

dots in the bottom row denote magnetite nanoparticles. The exploded views from the vials detail the filling state of the CNFs at that specific step. (Color figure online)

of samples were prepared. In one case, the nanoparticle-CNF dispersion was probe sonicated, while in the other, bath sonication was used keeping the sonication time fixed (~ 10 min). Figure 3a, b shows the difference in packing characteristics of nanoparticles inside CNFs prepared using probe sonication and bath sonication, respectively. Not surprisingly, probe sonication proved to be superior to bath sonication in terms of intercalation efficiency. HRTEM observations of the probe-sonicated samples showed that most of the open-ended tubes were densely packed with nanoparticles. On the other hand, most CNFs from the bath-sonicated samples were vacant, with nanoparticles mostly observed outside the CNFs. Few CNFs from the bath-sonicated sample revealed highly localized, small particle clusters inside their cavity. As compared to bath sonication, probe sonication has

much higher energy density, thus creating more rapid mixing of nanoparticles and CNFs in the suspension. This increases the probability of collisions of nanoparticles with the CNF open ends, and ultimately helps the particles to invade the cavity. At the same time, because of the higher energy density of probe sonication, there is higher probability for the liquid medium to wet the interior of the CNFs throughout their length, thus indirectly helping intercalate more nanoparticles. On the other hand, energetically intense probe sonication results in higher adhesion of the nanoparticles on the CNF outer walls, thus making the washing step more difficult and time consuming. In turn, the longer sonication periods required to clean up the outer CNF walls also force out nanoparticles from inside the cavity. Bath sonication, due to its lower energy density, facilitates the final washing step by causing

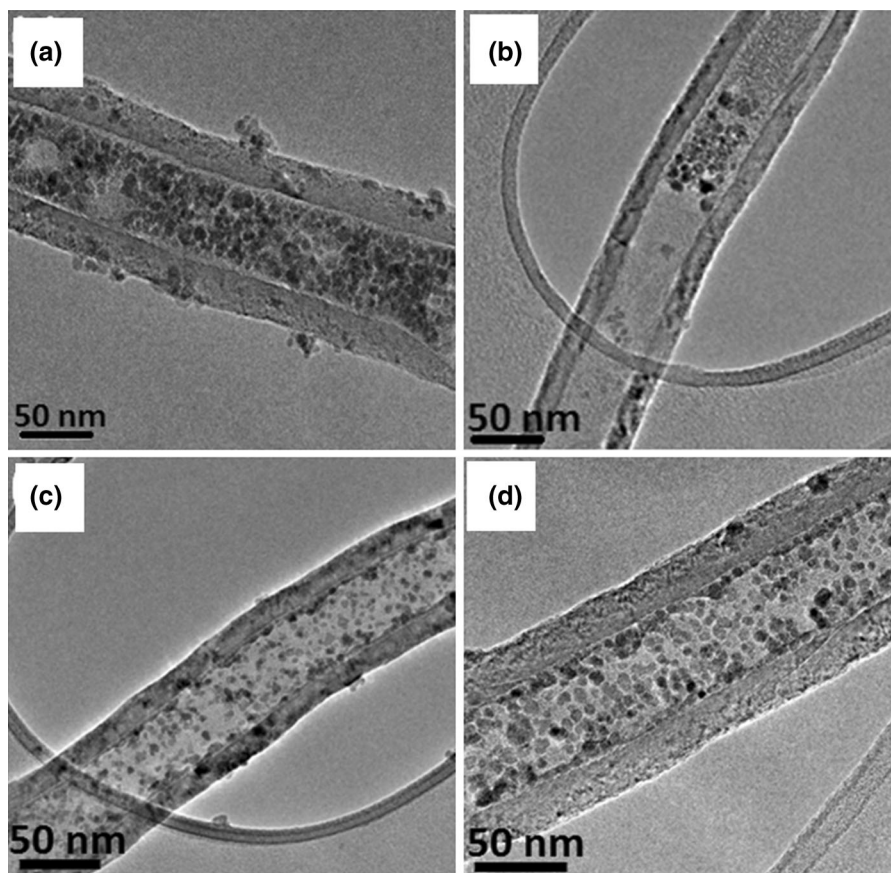


Fig. 3 Intercalated CNFs after 10 min of **a** probe sonication, and **b** bath sonication. **c, d** Intercalated CNFs after 1 and 6 h of bath sonication, respectively. The particle packing density rises with processing time (**b–d**)

relatively lower adhesion of the particles on the CNF outer walls.

Increased sonication times raised the number of intercalated nanoparticles and filled CNFs in both bath-sonicated and probe-sonicated samples. Figure 3c shows a representative filled CNF obtained after 1 h of bath sonication. The higher sonication time in this case increased the particle packing, as compared to CNFs obtained after 10 min of bath sonication (Fig. 3b). For even longer bath sonication times (6 h; Fig. 3d), the number of intercalated particles was further improved. In the 1 h-sonicated sample, approximately 80 % of the open-ended tubes contained nanoparticles. Almost all these CNFs had high intercalated particle density. In the 6 h sample, almost all open-ended CNFs with sufficiently large diameter (>35 nm) were densely packed with nanoparticles. Sonication processing time had similar

influence on the probe-sonicated samples, as confirmed by a separate set of experiments (see Supporting Information, Fig. S4) that varied sonication times from 10 s to 1,000 s.

The dense packing in Fig. 3c, d was seen throughout the entire CNF length. Hence, it was concluded that prolonged bath sonication facilitates higher nanoparticle intercalation and more uniform packing along the CNF length. This advantage, along with the looser adherence of nanoparticles on the CNF outer walls, made bath sonication more attractive as compared to probe sonication. Moreover, bath sonication had the advantage of being continuous, as contrasted with probe sonication where frequent interruptions were necessary to avoid dispersion overheating and premature loss of the host liquid.

The probability of nanoparticle intercalation into the CNF cavities increases with CNF-nanoparticle

collision probability. The number of collisions N (per unit volume) between nanoparticles and the open ends of the CNFs is estimated by (Chamberlain et al. 2010)

$$N = \alpha 4\pi D R_c n_1 n_2 \left[t + \frac{2R_c \sqrt{t}}{\sqrt{\pi D}} \right], \quad (1)$$

where D denotes the diffusion coefficient of nanoparticles, R_c the nanoparticle radius, n_1 and n_2 the nanoparticle and CNF concentrations in the liquid, t the time from the onset of the experiment, and $\alpha = 1/3$ (expression factor). D can be estimated by the Stokes–Einstein equation (Chamberlain et al. 2010)

$$D = \frac{kT}{6\pi\eta R_c}, \quad (2)$$

where k denotes Boltzmann's constant, T is the temperature, and η is the viscosity of the host liquid. Under simultaneous sonication of CNFs and nanoparticles, the interaction probability is expected to be orders of magnitude higher compared to the unaided diffusion case. In other words, the effective value of D for sonication-assisted simultaneous mixing would be much higher than the simple diffusive case. Moreover, prolonged bath sonication ensures uniform distribution of surfactant (present as a ferrofluid ingredient) and nanoparticles both inside and outside the CNF cavity. Prolonged sonication also helps the CNFs to mix well with the surfactant molecules, and to disperse efficiently, thus ensuring higher probability of nanoparticle–CNF interaction during the drying process. Because of the above reasons, simultaneous sonication of CNFs and nanoparticles yields higher intercalation efficiency and is thus preferable. This was also corroborated by the experiments, which showed that in the absence of this step, nanoparticle intercalation was significantly reduced (see Supporting Information, Fig. S5).

CNF:nanoparticle mass ratio and concentration of solids dispersed in solvent

Intercalation experiments were carried out with fixed CNF mass and varying nanoparticle amounts that corresponded to CNF:nanoparticle mass ratios of 10:4.16 and 10:1.04. Both samples were bath sonicated for 6 h. Subsequently, the standard drying and cleaning steps were performed. As the relative amount of nanoparticles decreased, the density of intercalated

nanoparticles decreased drastically (compare representative TEM images of Fig. 4a, b). This observation clearly shows the capability of the current method to control the number of intercalated magnetite nanoparticles inside the CNF cavity by changing the relative amount of nanoparticles with respect to the CNF content. Using this approach, CNFs with controlled magnetic properties can be fabricated, since such properties are expected to be proportional to the number of nanoparticles inside the CNF cavity.

The solids (CNF + nanoparticle) concentration in the liquid medium also influences the rheological properties of the dispersions. High solids concentration increases the viscosity or may alter the effective surface tension of the dispersion. Most importantly, as shown in Eq. 1, the collision frequency N depends on the concentrations of both CNFs and nanoparticles in dispersion, thus affecting the intercalation process. To investigate this effect, an additional experiment with 1 mg of CNFs and 0.416 mg of magnetite (supplied from EMG 911 ferrofluid) in the same amount of toluene and 6 h of bath sonication was carried out. The CNF:nanoparticle mass ratio was thus identical to the 10:4.16 case discussed above, but the solids concentration was 10 times smaller. Representative HRTEM images of cleaned (stripped of the particles deposited on the outer walls) samples are compared in Fig. 4a, c. As expected from Eq. 1, the probability of intercalation for higher solids concentration (Fig. 4a) is higher. For the low solids concentration, the interaction probability between CNFs and nanoparticles is relatively lower, thus contributing to lower nanoparticle packing overall. As shown in Fig. 4c, this packing is rather inhomogeneous, with most CNFs containing no particles over their length, except in a small fraction that contains densely packed clusters. Indeed, in the dispersion with lower solids content, CNF cavities were filled with toluene carrying fewer nanoparticles. After complete evaporation of the solvent outside the CNFs during drying, the toluene inside the CNF cavity also started to evaporate, thus shrinking in volume. In turn, capillary action collected the small number of nanoparticles into a shorter span of the CNF length, eventually concentrating them to very high packing over smaller portions of the CNF length (Fig. 4c). In this process, the edges of the densely packed nanoparticle cluster took the shape of the liquid meniscus, thus providing forensic evidence for the validity of the above mechanism. Consequently, for homogeneous

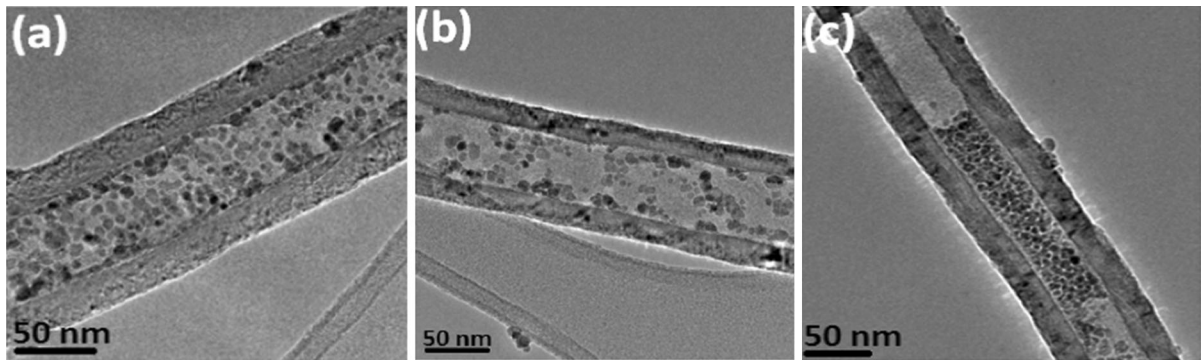


Fig. 4 Typical intercalated CNFs obtained from experiments that used dispersions comprising 10 mg CNF and **a** 4.16 mg nanoparticles, or **b** 1.04 mg nanoparticles (both supplied from EMG-911 ferrofluid). Image **c** shows intercalated CNFs

obtained using a dispersion with the same CNF:nanoparticle ratio as in **(a)**, but with solids concentration ten times lower than **(a)**. The solids concentration in **a** was ~ 0.1 wt%, while in **c** it was ~ 0.01 wt%

intercalation through the entire CNF length, the concentration of nanoparticles and CNFs into the liquid medium must be high enough (0.1 wt% in the present case).

Dispersion drying temperature

The present intercalation method is utilizing two important physical mechanisms to drive and encapsulate the nanoparticles inside the CNF cavities. The first mechanism relies upon the high energy density of sonication. The second mechanism aiding the intercalation process is the known (Bazilevsky et al. 2007, 2008) concentration-gradient-driven flow accomplished by evaporating the liquid dispersion medium either by heating (e.g., hot plate) or naturally at room temperature. Hence the drying temperature is expected to have significant influence on the intercalation mechanism. Important temperature-dependent properties, which may influence the intercalation process, are the diffusion coefficient of the nanoparticles, as well as the fluid properties and evaporation rate of the liquid medium. All prior experiments used 120 °C (drying temperature) for evaporating the liquid dispersion medium. One additional experiment was carried out where the dispersions were dried at room temperature. Representative images of the filled CNF samples are compared in Fig. 5. Figure 5a shows a typical CNF from the room temperature dried sample and reveals a smaller number of intercalated nanoparticles, as compared to the sample dried at 120 °C (Fig. 5c).

The denser particle packing attained with the higher drying temperature can be attributed to the corresponding stronger particle diffusion coefficient at that temperature. As per Eq. 2, apart from the proportional relationship between D and T , higher temperature also decreases the liquid viscosity, further raising diffusive agility, and in turn, facilitating the intercalation process during drying. In the room temperature dried sample, significant amounts of seemingly polymeric deposits were observed inside the CNF cavity (Fig. 5a); these deposits formed peapod-like morphologies, as reported elsewhere (Bazilevsky et al. 2007, 2008). In addition to nanoparticles and CNFs, surfactant molecules (fatty acids) were also present in the original ferrofluid dispersion. These surfactants also invade the CNFs during the drying/intercalation process and form deposit patterns such as those seen in between the particles in Fig. 5a. These deposits could not be seen in the 120 °C dried sample (Fig. 5c), thus suggesting that the higher drying temperature destroyed these surfactant remnants. To this end, the higher drying temperature offers the advantage of more pristine intercalated samples. Finally, careful inspection of Fig. 5a (see magnified detail in Fig. 5b) also reveals that multiple graphene layers peel off from the CNF wall and bend toward the polymeric deposit at the core of the CNF cavity. This peeling may be due to the capillary tension of the dispersion medium, which upon drying, forces the inner graphene layers of the CNF wall to separate out and bend toward the surfactant deposits. The protruding bent layers of graphene sheets were not observed in the sample dried

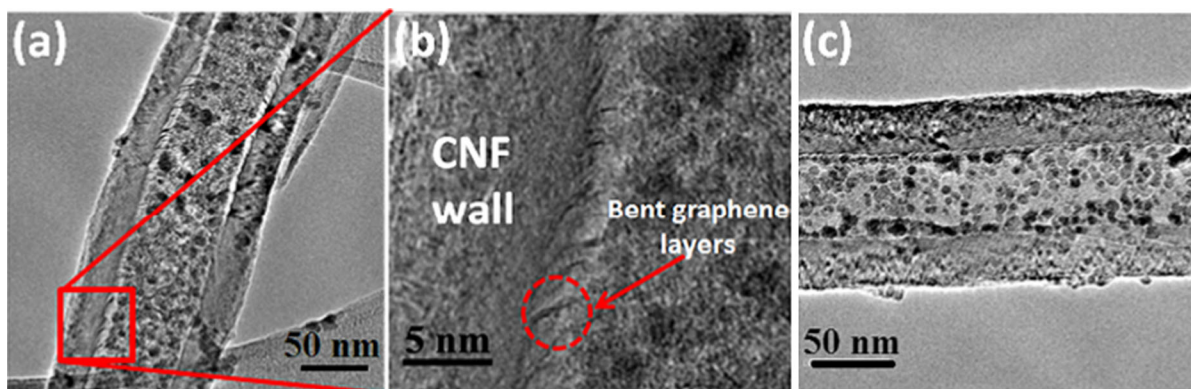


Fig. 5 Intercalated CNFs obtained after drying at **a** room temperature, and **c** 120 °C. Note the denser particle packing in **(c)**, as compared to **(a)**. **b** Magnified detail from **(a)** showing

bending of graphene sheets from CNF wall (*left*) toward the surfactant/nanoparticle mixture at the inner chamber of the CNF (*right*)

at 120 °C. It is worth noting that similar observations have been made (Ye et al. 2004) in the interior of hydrothermally synthesized closed-end carbon nanofibers which contained an aqueous phase. The capillary action of the enclosed water phase was reported therein to be responsible for the peeling of the graphene layers toward the encased fluid.

Magnetic properties of intercalated CNF powder and polymer composite films

The magnetite nanoparticles are single-domain crystallites which, due to their small size, are expected to be in the superparamagnetic regime at room temperature. Since, in the present case, the magnetic nanoparticles remain encased in the CNF cavity, the filled CNF vessels should retain, at first approximation, the magnetic character of the pristine magnetite nanoparticles within them. Indeed, as confirmed in Fig. 6, filled CNFs are superparamagnetic at room temperature with mean blocking temperature $T_B = 89.5$ K (Fig. 6a). Moreover, the magnetization curve measured at room temperature (Fig. 6b) presents no coercivity or remanence. The magnetic CNF saturation magnetization, $M_s = 14.3$ emu/gr (Fig. 6b), is of course lower than that of neat magnetite nanoparticles, due to the fractional presence of nanoparticles in the composite nanoparticle/CNFs system.

The presence of an external magnetic field would cause the induced magnetic moment of each entrapped nanoparticle to preferentially align parallel to the

field's direction, pulling them toward regions where the magnetic field is stronger. The magnitude of the magnetic force that each CNF experiences is proportional to the strength of the external magnetic field and the total number of nanoparticles encased inside the CNF. As shown in Fig. 7, the force of a standard magnetic bar (0.1 T) is high enough for the filled CNFs to overcome the liquid viscous drag and diffusive forces experienced in the liquid, and assemble onto the glass wall adjacent to the magnetic bar. This property is important because it can facilitate controlled positioning of the filled CNFs by means of external magnetic forces.

Intercalated CNFs with superparamagnetic properties, if dispersible in organic nonpolar solvents to facilitate their incorporation in polymeric systems, can be an asset for various technological applications. As an example, polymeric nanocomposite films can be formed by combining the magnetic and conductive properties of the intercalated CNFs with the mechanical flexibility and processability of polymers. To provide proof of concept, 40- μm -thick nanocomposite films were fabricated containing 7.2 wt% magnetic CNFs in poly(methyl methacrylate) (PMMA). As shown in Fig. 8a, the nanocomposite films attain magnetic properties, maintaining the room temperature superparamagnetic behavior of the magnetic CNFs, with similar mean blocking temperature. At the same time, the films are also electrically conducting due to the presence of the conductive CNFs. Figure 8b presents the linear Ohmic I–V behavior of the CNF/PMMA/ Fe_3O_4 nanocomposite film. The DC

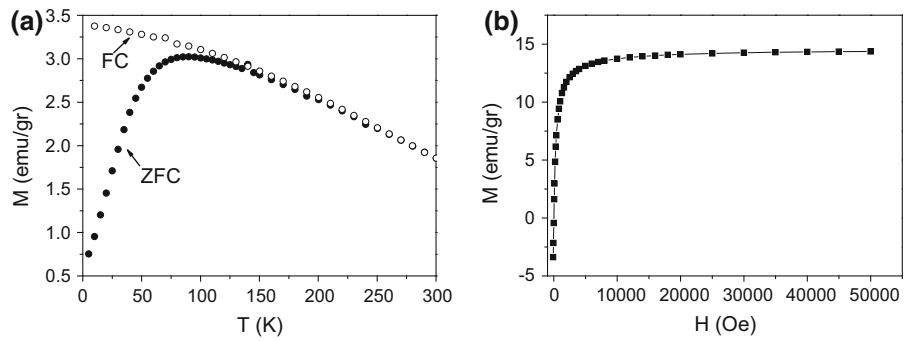


Fig. 6 **a** ZFC/FC magnetization curves, and **b** magnetization curve at 300 K of magnetite-intercalated CNF powder. The magnetization values have been normalized by the total mass of the CNF fibers

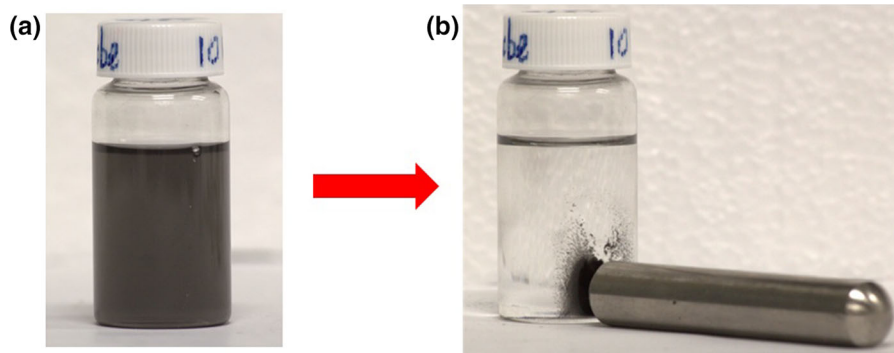


Fig. 7 **a** Well-dispersed magnetic CNFs in toluene; **b** CNFs move in the liquid and assemble on the glass vial wall closest to the adjacent magnetic bar (0.1 T)

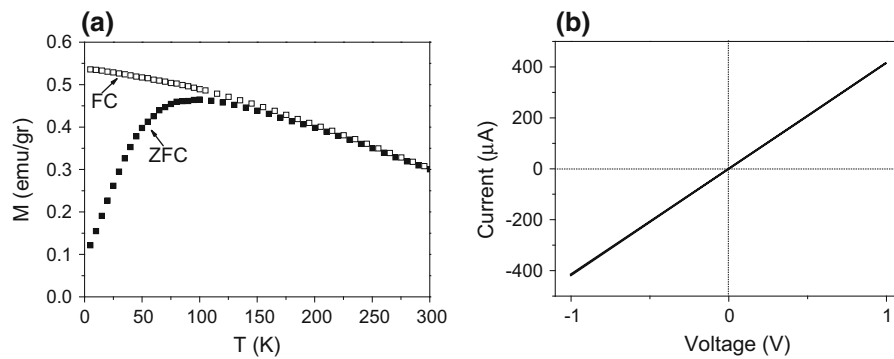


Fig. 8 **a** ZFC/FC magnetization curves of a 40- μm -thick composite film containing 7.2 wt% of magnetic CNFs distributed in a PMMA matrix. The magnetization values are

normalized with respect to the total weight of the nanocomposite film. **b** DC current-voltage (I - V) characteristic curve for the same film

electrical conductivity of the film is $\sigma = 10.22 \pm 3.42$ S/m, as calculated by $\sigma = t l d/R$, where t is the thickness of the film, l is the length of the electrodes used, d is the distance between them, and R is the slope of the data presented in Fig. 8b. The magnetic and electro-conducting properties of this thin composite film offer one example of multifunctionality of materials that can be fabricated with the present method. Such films could be of value in applications where simultaneous electrical and/or magnetic properties are required (e.g., electromagnetic interference shielding, etc.).

Conclusion

We have demonstrated a mild-temperature, nonchemical process to fabricate magnetically active and electro-conducting CNFs. CNF powders were produced by intercalating superparamagnetic, single-crystal, magnetite nanoparticles inside the CNF hollow cavities by sonication-assisted capillary imbibition and concentration-driven diffusion acting during the solvent evaporation stage. The influence of several important process parameters—such as sonication type and time, CNF-to-nanoparticle ratio and drying temperature—on intercalation efficiency (evaluated in terms of particle packing in the CNF cavities) was examined. We have shown that by tuning the process parameters, different nanoparticle packing densities can be obtained in the CNFs. The unique functionalities of the produced CNF powders offer rich technological opportunities. As an example, we have shown these active CNFs to be promising fillers for fabricating smart polymer nanocomposite thin films with simultaneous magnetic and electro-conductive properties. Such multifunctional composite materials can find applications in sensors, opto-electronic devices, energy and heat transfer devices, etc. Using the present method, it is feasible to intercalate multiple nanomaterials into the hollow CNF cavities, with each component adding a distinct functionality. Thus, the method is well suited for the fabrication of previously unattainable materials (e.g., metamaterials) and offers an attractive platform for studying fundamental properties of nanoparticles packed tightly in nanoenclosures.

Acknowledgments This material is based upon work supported in part by the US National Science Foundation under Grant NIRT CBET 0609062. MR was supported by a

CIES Fulbright Fellowship. The authors thank Dr. V. Caramia for assistance with the conductivity measurements and Dr. I.S. Bayer for fruitful discussions. Both are with the Istituto Italiano di Tecnologia, Genova, Italy.

References

- Ajayan PM, Iijima S (1993) Capillarity-induced filling of carbon nanotubes. *Nature* 361:333–334
- Al-Saleh MH, Sundararaj U (2009) A review of vapor grown carbon nanofiber/polymer conductive composites. *Carbon* 47:2–22
- Bachtold A, Hadley P, Nakanishi T, Dekker C (2001) Logic circuits with carbon nanotube transistors. *Science* 294:1317–1320
- Bazilevsky AV, Sun K, Yarin AL, Megaridis CM (2007) Selective intercalation of polymers in carbon nanotubes. *Langmuir* 23:7451–7455
- Bazilevsky AV, Sun K, Yarin AL, Megaridis CM (2008) Room-temperature, open-air, wet intercalation of liquids, surfactants, polymers and nanoparticles within nanotubes and microchannels. *J Mater Chem* 18:696–702
- Brune H, Ernst H, Grunwald A, Grünwald W (2006) Nanotechnology: assessment and perspectives. *Eth Sci Technol Assess* vol 27, Springer, Berlin Heidelberg
- Castillejos E, Debouttière P-J, Roiban L et al (2009) An efficient strategy to drive nanoparticles into carbon nanotubes and the remarkable effect of confinement on their catalytic performance. *Angew Chem Int Ed Engl* 48:2529–2533
- Chamberlain TW, Popov AM, Knizhnik AA et al (2010) The role of molecular clusters in the filling of carbon nanotubes. *ACS Nano* 4:5203–5210
- Charlier J, Lambin P, Ebbesen T (1996) Electronic properties of carbon nanotubes with polygonized cross sections. *Phys Rev B* 54:R8377–R8380
- Cheng H, Qiu H, Zhu Z et al (2012) Investigation of the electrochemical behavior of dopamine at electrodes modified with ferrocene-filled double-walled carbon nanotubes. *Electrochim Acta* 63:83–88
- Chou SY, Wei MS, Krauss PR, Fischer PB (1994) Single-domain magnetic pillar array of 35 nm diameter and 65 Gbits/in. 2 density for ultrahigh density quantum magnetic storage. *J Appl Phys* 76:6673–6675
- Chu A, Cook J, Heesom RJR et al (1996) Filling of carbon nanotubes with silver, gold, and gold chloride. *Chem Mater* 8:2751–2754
- Costa PMFJ, Coleman KS, Green MLH (2005) Influence of catalyst metal particles on the hydrogen sorption of single-walled carbon nanotube materials. *Nanotechnology* 16:512–517
- Dai H, Kong J, Zhou C et al (1999) Controlled chemical routes to nanotube architectures, physics, and devices. *J Phys Chem B* 103:11246–11255
- Day TM, Unwin PR, Wilson NR, Macpherson JV (2005) Electrochemical templating of metal nanoparticles and nanowires on single-walled carbon nanotube networks. *J Am Chem Soc* 127:10639–106447
- Day TM, Unwin PR, Macpherson JV (2007) Factors controlling the electrodeposition of metal nanoparticles on pristine single walled carbon nanotubes. *Nano Lett* 7:51–57

- Demoncey N, St O, Brun N et al (1998) Filling carbon nanotubes with metals by the arc-discharge method: the key role of sulfur. *Eur Phys J B* 4:147–157
- Dong X, Fu D, Ahmed MO et al (2007) Heme-enabled electrical detection of carbon monoxide at room temperature using networked carbon nanotube field-effect transistors. *Chem Mater* 19:6059–6061
- Dong X, Lau CM, Lohani A et al (2008) Electrical detection of femtomolar DNA via gold-nanoparticle enhancement in carbon-nanotube-network field-effect transistors. *Adv Mater* 20:2389–2393
- Dresselhaus M., Dresselhaus G., Avouris P. (2001) Carbon Nanotubes: Synthesis, Properties and Applications. *Top Appl Phys*, vol 80. Springer, Berlin
- Ebbesen W (1996) Wetting, filling and decorating. *J Phys Chem Solids* 57:951–955
- Erb RM, Libanori R, Rothfuchs N, Studart AR (2012) Composites reinforced in three dimensions by using low magnetic fields. *Science* 335:199–204
- Fragouli D, Buonsanti R, Bertoni G et al (2010) Dynamical formation of spatially localized arrays of aligned nanowires anisotropy. *ACS Nano* 4:1873–1878
- Fragouli D, Das A, Innocenti C, Guttigonta Y, Rahman S, Liu L, Caramia V, Megaridis CM, Athanassiou A (2014) Polymeric films with electric and magnetic anisotropy due to magnetically assembled functional nanofibers. *ACS Appl Mater Interfaces* 6:4535–4541
- Gautam UK, Costa PMFJ, Bando Y et al (2010) Recent developments in inorganically filled carbon nanotubes: successes and challenges. *Sci Technol Adv Mater* 11:054501
- Goldstein AN, Echer CM, Alivisatos AP (1992) Melting in semiconductor nanocrystals. *Science* 256:1425–1427. doi:10.1126/science.256.5062.1425
- Guan L, Shi Z, Li M, Gu Z (2005) Ferrocene-filled single-walled carbon nanotubes. *Carbon* 43:2780–2785
- Guerretpiecourt C, Le bouar Y, Loiseau A, Pascard H (1994) Relation between metal electronic structure and morphology of metal compounds inside carbon nanotubes. *Nature* 372:761–765
- Kornev KG, Halverson D, Korneva G et al (2008) Magnetostatic interactions between carbon nanotubes filled with magnetic nanoparticles. *Appl Phys Lett* 92:233117
- Korneva G, Ye H, Gogotsi Y et al (2005) Carbon nanotubes loaded with magnetic particles. *Nano Lett* 5:879–884
- Kuzmany H, Fink J, Mehring M, Roth S (2001) Nanotube. Electronic properties of molecular nanostructures. AIP-Press, Springer, New York, pp 562–567
- La Torre A, Rance GA, El Harfi J et al (2010) Transport and encapsulation of gold nanoparticles in carbon nanotubes. *Nanoscale* 2:1006–1010
- La Torre A, Fay MW, Rance GA et al (2012) Interactions of gold nanoparticles with the interior of hollow graphitized carbon nanofibers. *Small* 8:1222–1228
- Lee J, Park J, Kim J, Yi W (2008) Efficient visible photoluminescence from encapsulation of fluorescent materials inside single-walled carbon nanotubes. *Colloids Surf A* 313–314:296–299
- Li L-J, Khlobystov AN, Wiltshire JG et al (2005) Diameter-selective encapsulation of metallocenes in single-walled carbon nanotubes. *Nat Mater* 4:481–485
- Liu C, Fan YY, Liu M et al (1999) Hydrogen storage in single-walled carbon nanotubes at room temperature. *Science* 286:1127–1129
- Luo J, Mark LP, Giannakopoulos AE et al (2011) Field ionization using densely spaced arrays of nickel-tipped carbon nanotubes. *Chem Phys Lett* 505:126–129
- Misewich JA, Martel R, Avouris P, Tsang JC, Heinze S, Tersoff J (2003) Electrically induced optical emission from a carbon nanotube FET. *Science* 300:783–786
- Mönch I, Meyer A, Leonhardt A et al (2005) Ferromagnetic filled carbon nanotubes and nanoparticles: synthesis and lipid-mediated delivery into human tumor cells. *J Magn Magn Mater* 290–291:276–278
- Okazaki T, Suenaga K, Hirahara K et al (2001) Communications to the editor. *J Am Chem Soc* 123:9673–9674
- Palaniselvam T, Kannan R, Kurungot S (2011) Facile construction of non-precious iron nitride-doped carbon nanofibers as cathode electrocatalysts for proton exchange membrane fuel cells. *Chem Commun* 47:2910–2912
- Pan X, Bao X (2008) Reactions over catalysts confined in carbon nanotubes. *Chem Commun (Camb)* 47:6271–6281
- Pati SP, Bhushan B, Das D (2010) Exchange interaction at the interface of Fe–NiO nanocomposites. *J Solid State Chem* 183:2903–2909
- Pati SP, Kumar S, Das D (2012) Memory effects in exchange coupled Fe/Co₃O₄ nanocomposites. *Mater Chem Phys* 137:303–309
- Qiu H, Shi Z, Zhang S et al (2006) Synthesis and Raman scattering study of double-walled carbon nanotube peapods. *Solid State Commun* 137:654–657
- Sinha-Ray S, Sahu RP, Yarin AL (2011) Nano-encapsulated smart tunable phase change materials. *Soft Matter* 7:8823–8827
- Sloan J, Wright DM, Woo H-G et al (1999) Capillarity and silver nanowire formation observed in single walled carbon nanotubes. *Chem Commun* 8:699–700
- Smith BW, Monthieux M, Luzzi DE (1998) Encapsulated C60 in carbon nanotubes. *Nature* 396:323–324
- Smith BW, Monthieux M, Luzzi DE (1999) Carbon nanotube encapsulated fullerenes: a unique class of hybrid materials. *Chem Phys Lett* 315:31–36
- Sutradhar S, Mukhopadhyay K, Pati S, Das S, Das D, Chakrabarti PK (2013) Modulated magnetic property, enhanced microwave absorption and Mössbauer spectroscopy of Ni_{0.40}Zn_{0.40}Cu_{0.20}Fe₂O₄ nanoparticles embedded in carbon nanotubes. *J Alloys Compd* 576:126–133
- Takenobu T, Takano T, Shiraiishi M et al (2003) Stable and controlled amphoteric doping by encapsulation of organic molecules inside carbon nanotubes. *Nat Mater* 2:683–688
- Tessonnier J-P, Ersen O, Weinberg G et al (2009a) Selective deposition of metal nanoparticles inside or outside multi-walled carbon nanotubes. *ACS Nano* 3:2081–2089
- Tessonnier J-P, Rosenthal D, Girgsdies F, Amadou J et al (2009b) Influence of the graphitisation of hollow carbon nanofibers on their functionalisation and subsequent filling with metal nanoparticles. *Chem Commun* 46:7158–7160
- Tilmaiciu CM, Soula B, Galibert A-M et al (2009) Synthesis of superparamagnetic iron(III) oxide nanowires in double-walled carbon nanotubes. *Chem Commun* 43:6664–6666

- Tsang SC, Chen YK, Harris PJF, Green MLH (1994) A simple chemical method of opening and filling carbon nanotubes. *Nature* 372:159–162
- Ugarte D, Chatelain A, de Heer WA (1996) Nanocapillarity and chemistry in carbon nanotubes. *Science* 274:1889–1897
- Wang C, Guo S, Pan X et al (2008) Tailored cutting of carbon nanotubes and controlled dispersion of metal nanoparticles inside their channels. *J Mater Chem* 18:5782–5786
- Winkler A, Mühl T, Menzel S et al (2006) Magnetic force microscopy sensors using iron-filled carbon nanotubes. *J Appl Phys* 99:104905
- Wolny F, Mühl T, Weissker U et al (2010) Iron filled carbon nanotubes as novel monopole-like sensors for quantitative magnetic force microscopy. *Nanotechnology* 21:435501
- Ye H, Naguib N, Gogotsi Y et al (2004) Wall structure and surface chemistry of hydrothermal carbon nanofibres. *Nanotechnology* 15:232–236